GEOPHYSICS, VOL. 73, NO. 5 (SEPTEMBER-OCTOBER 2008); P. VE75–VE92, 16 FIGS.
10.1190/1.2953979

Anisotropic local tomography

Zvi Koren[1], Igor Ravve[1], Gladys Gonzalez[1], and Dan Kosloff[1,2]

ABSTRACT

Local tomography is interactive, ray-based, residual-interval-parameter analysis for updating background anisotropic velocity parameters. The method operates directly on image gathers generated by anisotropic curved-ray Kirchhoff time migration. A locally 1D, spatially varying, vertical transversely isotropic model is assumed. The background anisotropy parameters are the instantaneous (interval) vertical compression velocity V_P and the two Thomsen anisotropy parameters, δ and ε. The interval velocity δ is updated from short-offset reflection events, and ε is updated from available long-offset data. The medium parameters are updated from the top down both vertically and by layers, one parameter at a time. The picked residual-anisotropy parameters correspond to the residual-moveout (RMO) curves that best fit the migrated reflection events. The method is based on splitting the contribution to the computed RMO at a given point into two parts: from overburden residual parameters and from the actual picked residual parameter. This approach allows for direct residual-interval-parameter analysis to be applied in the same way we perform the commonly used residual-effective-parameter analysis. The local tomography enables a controlled interactive estimation of the long-wavelength anisotropy parameters. The reliable anisotropy parameters estimated by the local approach are used as a background (guiding) model for a global tomography. This makes it possible to successfully apply a global constrained inversion that is performed simultaneously for all parameters of all output intervals using detailed RMO information.

INTRODUCTION

The objective of anisotropic curved-ray local tomography is to update background anisotropic velocity parameters in vertical time. The tomography uses residual moveouts (RMOs) measured along image gathers generated by curved-ray Kirchhoff time migration. A vertical transversely isotropic (VTI) model is assumed. The background anisotropy parameters are the instantaneous (interval) vertical compression velocities V_P and the two Thomsen anisotropy parameters, ε and δ.

Seismic tomography is based on a linearized relation between traveltime errors measured along reflecting rays (RMOs) and model errors. Local tomography uses this linear relation for ray-based residual-parameter analysis. The medium parameters are updated from the top down both vertically and by layers, one parameter at a time, location by location. Residual-anisotropy parameters are picked interactively. The residual picks correspond to the RMO curves that best fit the migrated-reflection events. The analysis is performed for single locations and for a single parameter type (velocity, ε, or δ).

This approach can be considered a type of interactive coherency inversion analysis that is performed directly along the migrated image gathers. It is an attractive replacement for conventional analysis of effective anisotropic parameters (e.g., Alkhalifah, 1997a, 1997b). Effective parameters are model characteristics (normally two or three per reflection event) that describe the RMO of the reflected migrated events, e.g., rms velocity, fourth-order average velocity, or effective anellipticity. The inversion of the effective parameters into interval values, governed by the generalized Dix transform, is often an unstable approach and can lead to nongeologically plausible model parameters.

The advantage of the proposed method is that it directly estimates the interval model parameters, providing much better control over the validity and feasible range of the updated values. It is recommended that the analysis should be performed throughout selected sparse locations in which the RMOs are sensitive to model changes. This allows us to obtain long-wavelength and smooth updated parameters, avoiding unwanted artifacts and oscillations. The updated model can be used as the initial model for global tomography. Analysis can then be performed in batch mode for the whole layer, scanning residual-model parameters within a specified range. The output is a horizon-based semblance plot for a layer where maximum amplitudes indicate best-fit model perturbations.

Manuscript received by the Editor 9 January 2008; revised manuscript received 22 May 2008; published online 1 October 2008.
[1]Paradigm Geophysical, Herzliya, Israel. E-mail: zvi.koren@PDGM.com; igor.ravve@PDGM.com; gladys.gonzalez@PDGM.com.
[2]Tel Aviv University, Tel Aviv, Israel. E-mail: dan@seismo.tau.ac.il.

Because the 3D model is realized as a locally varying 1D medium, analysis is performed independently for each lateral location. The results are further smoothed for lateral continuity. Local tomography is based on special 3D ray tracing for the 1D anisotropic (VTI) model with flat or tilted reflectors. Obviously, use of this method is limited to areas with moderate lateral velocity variations, where the main assumption of a locally varying 1D medium is justified.

We describe a local tomographic tool that relates small variations of anisotropic model parameters to the residual traveltime. Each change in a parameter causes residual traveltime for a two-way (incident-reflected) raypath. We assume that, for zero offset, the incident and the reflected paths coincide; this is true for both the background and the updated models. However, because the background model satisfies imaging conditions, we assume that for zero offset the total traveltime is preserved — the zero-offset traveltime is the same for the background (unperturbed) and the updated (perturbed) models.

For a layer-based approach, the subsurface geologic model consists of a set of layers (formations) separated by interfaces (geologic horizons). The formation interfaces are reflection/transmission horizons. The distribution of anisotropic-medium parameters is assumed to be continuous and smooth within each layer and discontinuous at the transition zones along the interfaces. The variable model parameters are the interface locations and three VTI medium properties — the vertical compression velocity and two Thomsen anisotropy parameters, ε and δ — for a total of four parameters. However, because zero-offset traveltime is preserved, the errors of horizon locations are not independent values; they depend on the errors of the VTI-medium's properties. The perturbed-model parameters are defined at the layers between the horizons. The horizon locations are updated as the local tomography proceeds, along with updating the medium properties.

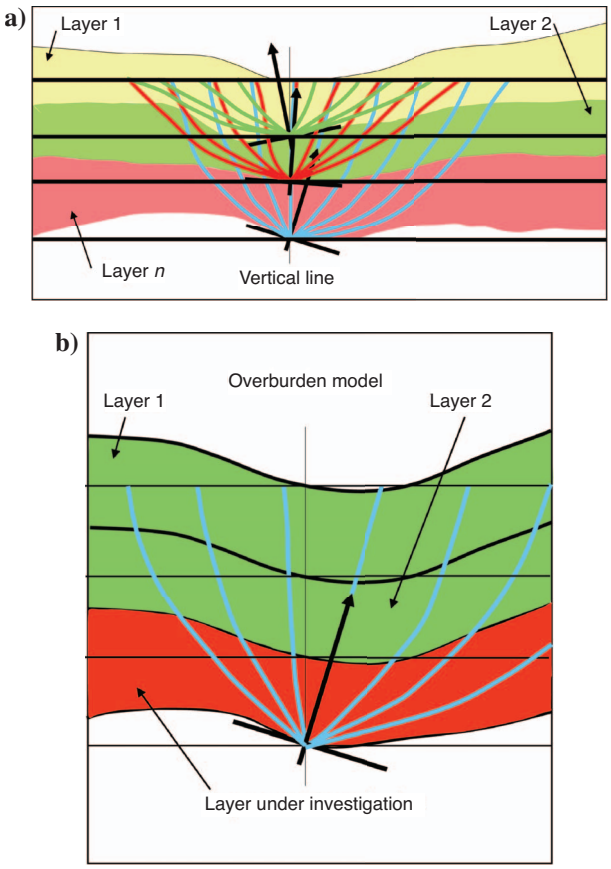

Figure 1. (a) Raypaths in tomographic analysis. The tilted reflectors are tangent to the horizons. Horizontal lines show the vertical locations of the reflection/transmission points in a locally 1D model. (b) Reflection and transmission horizons in local tomography analysis.

Seismic tomography is a nonlinear inverse problem (Tarantola, 1987; Menke, 1989) that is commonly solved iteratively by applying linear methods (e.g., Goldin, 1986). In global tomography methods, traveltime errors along reflected rays are minimized to find velocity-depth model parameters simultaneously (Bishop et al., 1985; Farra and Madariaga, 1988; Williamson, 1990; Stork, 1992; Kosloff et al., 1996). Ray tracing in the tomography requires instantaneous velocity, and the success of the tomography depends strongly on the initial instantaneous velocity field and anisotropy parameters, which are usually obtained by simplistic approximations. In this paper, we propose a fast, reliable anisotropic local tomography tool whose results may be used as an initial approximation for global tomography. It is an extension of earlier work (Koren et al., 2006), presented here in full with applications on real data.

THE METHOD

The input for local tomography is a background anisotropic velocity model and common image gathers (CIGs) generated by anisotropic curved-ray migration. Local tomography is a residual-parameter scanning tool, operating directly on migrated image gathers. The goal is to find the optimal residual-anisotropy parameters that correspond to the best fit of the reflection events on the image gathers. The workflow supports two alternative modes: (1) layer mode or layer-stripping approach, in which the analysis is performed layer by layer for different lateral locations and (2) vertical mode, in which the analysis is performed location by location, from the top down, for a set of points (local reflecting surfaces) located along the vertical line.

Local tomography analysis is based on interactive ray tracing, which is performed through the background model from each analyzed point up to the surface for the set of offsets and azimuths indicated by the migrated gather (Figure 1a). The black, solid horizontal lines in Figure 1a show the vertical locations of horizons at the lateral location of the image point (reflection point). The model is locally one dimensional; for all rays — irrespective of at which lateral coordinates the rays intersect the horizons — the vertical locations of the horizons are the same. The tilted reflectors or transmission surfaces are tangent to the horizons at the lateral location of the reflection point. Here, rays with different offsets intersect a tilted horizon at different lateral locations; therefore, the vertical locations of the transmission points are also different. However, in the computational scheme for a locally 1D model, these vertical locations are assumed to be the same.

Tomographic coefficients are computed along the rays. The parameters are studied one at a time: residuals of the axial compression velocity ΔV_P, Thomsen parameter $\Delta\delta$, or Thomsen parameter $\Delta\varepsilon$. Traveltime errors along the rays are a function of the picked residual model parameters and consist of two parts: traveltime errors from overburden residual parameters and from the analyzed layer (interval), as shown in Figure 1b. The first part is computed once (while tracing the rays) because the overburden residual parameters have already been picked and are assumed to be fixed within the actual analysis. The second part is computed for each scanned residual pa-

rameter. For each traveltime error or RMO curve, a coherency measure (semblance) is computed within a given time (or depth) window. The residual model parameter that corresponds to the highest semblance value is selected (picked).

This traveltime-splitting approach is the core of our method. It enables the performance of residual-interval-parameter analysis along the whole model for all layers, eliminating the need to remigrate the data when moving from layer to layer. Residual-interval-parameter analysis is performed in the same fashion as commonly used residual-effective-parameter analysis.

The linearized dependency between residual traveltime and residual-model parameters is a basic tomographic assumption; therefore, several iterations generally are needed to solve the nonlinear local tomography problem. After each iteration, the anisotropic velocity model is updated with the picked residual parameters and a new anisotropic migration is performed.

VTI PARAMETERS AND THEIR RANGE

Although the VTI medium is described by five Thomsen (1986) parameters, only four parameters are needed to study compressional waves. Furthermore, the ratio between the vertical compression and shear velocities, V_P and V_S, is assumed to be constant because it has a very minor effect on the phase velocity (Tsvankin, 2001):

$$\frac{V_S}{V_P} = \frac{1}{2}, \quad f \equiv 1 - \frac{V_S^2}{V_P^2} = \frac{3}{4}. \tag{1}$$

This leaves three variable parameters: V_P, δ, and ε. The limits for δ depend on the ratio f (Tsvankin, 2001):

$$\delta^{\min} = -\frac{f}{2} = -\frac{3}{8}, \quad \delta^{\max} = \frac{2(1-f)}{f} = \frac{2}{3}. \tag{2}$$

In practice, we maintain a narrower range: $-0.2 \le \delta \le 0.5$. The second Thomsen parameter ε is theoretically limited only from below. Laboratory and field data indicate the velocity in the isotropy plane (horizontal velocity) is usually larger than V_P. This means ε is positive, and we accept the range $0 \le \varepsilon \le 0.5$.

ANISOTROPIC RAY TRACING

Ray tracing is a core element of seismic tomography. In a 1D medium, the horizontal slowness of the ray is constant. We distinguish between initial-value ray tracing (IVRT) and boundary-value ray tracing (BVRT). IVRT considers a single ray with a given horizontal slowness and vertical time at the starting point. The goal of BVRT is to find the parameters of a specific ray pair (incident and reflected rays) with a given offset and azimuth on the earth's surface. BVRT is explained in Appendix A. Throughout this study, we assume, for the sake of symmetry, that both rays emerge from the earth's surface and arrive at the image point.

INITIAL-VALUE RAY TRACING

In a 1D model, IVRT is two-dimensional. The raypath is a curved line within a unique vertical plane. Let h be the horizontal coordinate in this plane. The vertical coordinate is depth z or vertical time t_0. The vertical time is defined by

$$dt_0 = \frac{dz}{V_P(t_0)}. \tag{3}$$

Tracing is done numerically by solving a set of ordinary differential equations (ODEs). The governing function is the Hamiltonian, which depends on two slowness components — horizontal p_h and vertical p_z — and on the properties of the medium, which in turn depend only on vertical time t_0. Vertical time is an independent variable, and depth can be obtained by integration.

Recall that in the 1D model, the medium properties are assumed (locally) to be laterally invariant; therefore, the horizontal slowness does not change along the ray, $p_h = \text{const}$ (thus, p_h can be used as a ray parameter). The Hamiltonian function that follows from the Christoffel equation for P-SV-waves (e.g., Tsvankin, 2001) reads

$$G(p_h, p_z, z) = \frac{K - L \cdot V_P^2 - V_P^{-2}}{2f}, \tag{4}$$

where parameters K and L are

$$\begin{aligned} K &= (2-f)\cdot(p_h^2 + p_z^2) + 2\varepsilon p_h^2, \\ L &= (1-f)\cdot(p_h^2 + p_z^2)^2 + 2\varepsilon p_h^2[(1-f)p_h^2 + p_z^2] \\ &\quad - 2\delta f p_h^2 p_z^2. \end{aligned} \tag{5}$$

The Hamiltonian vanishes at any point along the ray. The resolving ray-tracing equations include two equations for the raypath,

$$\frac{dh}{d\sigma} = \frac{\partial G}{\partial p_h}, \quad \frac{dz}{d\sigma} = \frac{\partial G}{\partial p_z}, \tag{6}$$

and an equation for vertical slowness,

$$\frac{dp_z}{d\sigma} = -\frac{\partial G}{\partial z}, \quad p_h(\sigma) = \text{const}, \tag{7}$$

with

$$\frac{\partial G}{\partial z} = \frac{\partial G}{\partial t_0}\cdot\frac{dt_0}{dz} = \frac{1}{V_P}\cdot\frac{\partial G}{\partial t_0}, \tag{8}$$

where σ is an independent integration parameter. We assume $f = \text{const}$, so the vertical time derivative $\partial G/\partial t_0$ comprises three terms:

$$\frac{\partial G}{\partial t_0} = \frac{\partial G}{\partial V_P}\cdot\frac{dV}{dt_0} + \frac{\partial G}{\partial \delta}\cdot\frac{d\delta}{dt_0} + \frac{\partial G}{\partial \varepsilon}\cdot\frac{d\varepsilon}{dt_0}. \tag{9}$$

The derivatives of the Hamiltonian with respect to the medium properties are

$$\begin{aligned} \frac{\partial G}{\partial V_P} &= \frac{2}{fV_P^3} - \frac{2\varepsilon p_h^2}{fV_P} - \frac{2-f}{f}\cdot\frac{p_h^2 + p_z^2}{V_P}, \\ \frac{\partial G}{\partial \delta} &= p_h^2 p_z^2 \cdot V_P^2, \\ \frac{\partial G}{\partial \varepsilon} &= \frac{p_h^2}{f} - \frac{(1-f)p_h^2 + p_z^2}{f}\cdot p_h^2 \cdot V_P^2. \end{aligned} \tag{10}$$

Finally, we replace the second equation of set 6 by

$$\frac{dt_0}{d\sigma} = \frac{dt_0}{dz}\cdot\frac{dz}{d\sigma} = \frac{\dfrac{\partial G}{\partial p_z}}{V_P}. \quad (11)$$

Note that vertical slowness along the raypath can be defined not only from equation 8 but also from the vanishing Hamiltonian:

$$G(p_h,p_z) = 0, \quad (12)$$

where the horizontal slowness p_h is a known constant value.

The solution of equation 12 for p_z is exact and free from discrepancies that occur with the numerical integration of ODE 7. However, the exact solution defines only the absolute value of p_z, and equation 7 is still needed to determine the change in the vertical slowness sign, which occurs for turning rays.

ARC LENGTH AND TRAVELTIME

The arc-length increment is defined by

$$dl = \sqrt{dh^2 + dz^2}, \quad (13)$$

so the arc-length derivative becomes

$$\frac{dl}{d\sigma} = \sqrt{\left(\frac{dh}{d\sigma}\right)^2 + \left(\frac{dz}{d\sigma}\right)^2}. \quad (14)$$

Taking into account ray-tracing equation 6, we obtain

$$\frac{dl}{d\sigma} = \sqrt{\left(\frac{\partial G}{\partial p_h}\right)^2 + \left(\frac{\partial G}{\partial p_z}\right)^2}. \quad (15)$$

The traveltime derivative can be obtained with the chain rule:

$$\frac{dt}{d\sigma} = \frac{\partial t}{\partial h}\cdot\frac{dh}{d\sigma} + \frac{\partial t}{\partial z}\cdot\frac{dz}{d\sigma}. \quad (16)$$

Introducing equation 6 into 16 results in

$$\frac{dt}{d\sigma} = \frac{\partial G}{\partial p_h}\cdot p_h + \frac{\partial G}{\partial p_z}\cdot p_z. \quad (17)$$

The traveltime and raypath length are integrated, along with solving the basic ODE set.

TOMOGRAPHIC COEFFICIENTS FOR MEDIUM PROPERTIES

Tomographic coefficients relate small perturbations of medium properties and displacements of horizons to traveltime errors along specular rays. The relationship between the traveltime error and medium-property residuals is derived in Appendix B. To obtain the residual traveltime caused by variations in the medium properties, we integrate infinitesimal variations of traveltime along the raypath. The raypath can be divided into a number of intervals (layers); at each interval, the residuals of the medium properties are assumed to be constant:

$$\Delta t^{\text{medium}} = \sum_k \Delta t_k^{\text{medium}}, \quad (18)$$

where k is the layer index. For each individual layer k, the residual traveltime becomes

$$\Delta t_k^{\text{medium}} = -\Delta V_k\cdot\int_{\sigma_k}\frac{\partial G}{\partial V_P}d\sigma - \Delta\delta_k\cdot\int_{\sigma_k}\frac{\partial G}{\partial \delta}d\sigma - \Delta\varepsilon_k\cdot\int_{\sigma_k}\frac{\partial G}{\partial \varepsilon}d\sigma. \quad (19)$$

Tomographic coefficients are defined as derivatives of traveltime with respect to the model-parameter variations:

$$A_k^V = \frac{\partial \Delta t_k^{\text{medium}}}{\partial \Delta V_P}, \quad A_k^\delta = \frac{\partial \Delta t_k^{\text{medium}}}{\partial \Delta \delta}, \quad A_k^\varepsilon = \frac{\partial \Delta t_k^{\text{medium}}}{\partial \Delta \varepsilon}. \quad (20)$$

Thus,

$$A_k^V = -\int_{\sigma_k}\frac{\partial G}{\partial V_P}d\sigma, \quad A_k^\delta = -\int_{\sigma_k}\frac{\partial G}{\partial \delta}d\sigma, \quad A_k^\varepsilon = -\int_{\sigma_k}\frac{\partial G}{\partial \varepsilon}d\sigma, \quad (21)$$

where the integration is performed in the background medium along the ray-pair trajectory. With the tomographic coefficients defined above, the residual traveltime can be presented as

$$\Delta t_k^{\text{medium}} = \sum_k A_k^V\cdot\Delta V_k + \sum_k A_k^\delta\cdot\Delta\delta_k + \sum_k A_k^\varepsilon\cdot\Delta\varepsilon. \quad (22)$$

Equation 22 is valid for a given specific trajectory of the ray pair.

Note that equation 21 can be arranged in the form of an ODE set:

$$\frac{dA^V}{d\sigma} = -\frac{\partial G}{\partial V_P}, \quad \frac{dA^\delta}{d\sigma} = -\frac{\partial G}{\partial \delta}, \quad \frac{dA^\varepsilon}{d\sigma} = -\frac{\partial G}{\partial \varepsilon}. \quad (23)$$

Equation set 23 presents three additional ODEs, which are integrated along with the basic ray tracing and with calculating the traveltime and arc length. The tomographic coefficients take virtual variations in the medium properties into account but do not yet account for possible horizon shifts.

SHIFT OF REFLECTION POINT IN DEPTH

Two factors cause traveltime variations: residuals of medium properties and a shift of the reflection points in depth (Koren et al., 1999). The tomographic coefficient related to the vertical shift of the reflection horizon is defined as

$$A_z^{\text{horizon}} = \frac{\partial \Delta t^{\text{horizon shift}}}{\partial z}. \quad (24)$$

This coefficient depends on the vertical components of incident and reflected ray slowness p_z^{in} and p_z^{re}, respectively (see Appendix C):

$$A_z^{\text{horizon}} = p_z^{\text{horizon}}, \quad \text{where } p_z^{\text{horizon}} = p_z^{\text{in}} + p_z^{\text{re}}. \quad (25)$$

For this study, we accept the convention that the two rays arrive at the reflection point.

We assume that zero-offset traveltime is preserved. As the medium properties change, the depth of the reflection point varies accordingly. Let $\Delta t^{\text{medium}}_{\text{zero offset}}$ be the one-way zero-offset traveltime change caused only by the medium-property variation. This can be established by applying equation 22 to the zero-offset ray. Let Δz be the change of depth at the reflection point. The variation of traveltime $\Delta t^{\text{horizon shift}}_{\text{zero offset}}$ caused solely by this vertical shift is

$$\begin{aligned}\Delta t^{\text{horizon shift}}_{\text{zero offset}} &= \Delta t^{\text{horizon shift},S}_{\text{zero offset}} + \Delta t^{\text{horizon shift},R}_{\text{zero offset}} \\ &= \Delta z \cdot p_z^{\text{horizon}},\end{aligned} \quad (26)$$

where p_z^{horizon} is defined in equation C-2 (Appendix C). Superscript S is related to the incident ray; superscript R, to the reflected ray. For zero offset, the two rays coincide, and the increase or decrease of traveltime because of the horizon shift is the same for both rays:

$$\Delta t^{\text{horizon shift},S}_{\text{zero offset}} = \Delta t^{\text{horizon shift},R}_{\text{zero offset}}. \quad (27)$$

In addition, for zero-offset rays,

$$p_z^{\text{horizon}} = p_z^{\text{in}} + p_z^{\text{re}} = 2p_z^{\text{zero offset}}. \quad (28)$$

Conservation of the two-way zero-offset traveltime reads

$$\Delta t^{\text{horizon shift}}_{\text{zero offset}} = -2\Delta t^{\text{medium}}_{\text{zero offset}} \quad (29)$$

or

$$\Delta z \cdot p_z^{\text{zero offset}} = -\Delta t^{\text{medium}}_{\text{zero offset}}. \quad (30)$$

This yields an explicit expression of the reflector-depth variation:

$$\Delta z = \frac{1}{p_z^{\text{zero offset}}} \times \sum_{k=1}^{N} \int_{\sigma_k} \underbrace{\left(\frac{\partial G}{\partial V_{\text{P}}}\Delta V_k + \frac{\partial G}{\partial \delta}\Delta\delta_k + \frac{\partial G}{\partial \varepsilon}\Delta\varepsilon_k\right)}_{\text{zero offset}} d\sigma. \quad (31)$$

Variation of depth Δz is the same for all offsets. However, the change in traveltime caused by this variation differs for different offsets i:

$$\begin{aligned}\Delta t_i^{\text{horizon}} &= p_{z,i}^{\text{horizon}}\Delta z \\ &= \frac{p_{z,i}^{\text{in}} + p_{z,i}^{\text{re}}}{p_z^{\text{zero offset}}} \\ &\quad \times \sum_{k=1}^{N} \int_{\sigma_k} \underbrace{\left(\frac{\partial G}{\partial V}\Delta V_k + \frac{\partial G}{\partial \delta}\Delta\delta_k + \frac{\partial G}{\partial \varepsilon}\Delta\varepsilon_k\right)}_{\text{zero offset}} d\sigma.\end{aligned} \quad (32)$$

FULL TOMOGRAPHIC COEFFICIENTS

With equation 32, we can obtain the tomographic coefficients that account for the medium property variation and horizon shifts:

$$\begin{aligned}A_{i,k}^m = &-\underbrace{\int_{\sigma_k} \frac{\partial G}{\partial m} d\sigma}_{\substack{\text{incident ray,}\\ \text{offset } i}} - \underbrace{\int_{\sigma_k} \frac{\partial G}{\partial m} d\sigma}_{\substack{\text{reflected ray,}\\ \text{offset } i}} \\ &+ \frac{p_z^{\text{in}} + p_z^{\text{re}}}{p_z^{\text{zero offset}}} \cdot \underbrace{\int_{\sigma_k} \frac{\partial G}{\partial m} d\sigma}_{\text{zero offset ray}},\end{aligned} \quad (33)$$

where m is the parameter type that should be replaced by a variable medium property,

$$m = \{V, \delta, \varepsilon\} \quad \text{and } A_k^m = \{A_k^V, A_k^\delta, A_k^\varepsilon\}, \quad (34)$$

k is the layer index, and i is the offset index. Equation 33 is actually a set of three equations. After ray tracing is done, $A_{i,k}^V$, $A_{i,k}^\delta$, $A_{i,k}^\varepsilon$ are known values along the rays. For any offset i, the two-way residual traveltime includes the contribution of the overburden layers and that of the current layer,

$$\Delta t_i = \Delta t_i^{\text{overburden}} + \Delta t_i^{\text{current layer}}, \quad (35)$$

where the effect of the overburden is

$$\Delta t_i^{\text{overburden}} = \sum_{k=1}^{N-1} A_{i,k}^V \Delta V_k + A_{i,k}^\varepsilon \Delta\varepsilon_k + A_{i,k}^\delta \Delta\delta_k, \quad (36)$$

the effect of the current layer is

$$\Delta t_i^{\text{current layer}} = A_{i,N}^V \Delta V_N + A_{i,N}^\varepsilon \Delta\varepsilon_N + A_{i,N}^\delta \Delta\delta_N, \quad (37)$$

and N is the total number of layers, including the current layer. Equations 36 and 37 express the linearized relationship between the model parameter perturbations and the residual traveltime.

SINGLE-PARAMETER SCANNING

Local tomography is a layer-stripping approach performed for single locations and for a single parameter type m. This approach is an interactive coherency-inversion analysis performed directly along migrated image gathers (Koren et al., 1999, 2006). It is recommended to first select sparse locations along the layer where the RMOs are sensitive to the model changes. The analysis can then be performed in batch mode for the whole layer, scanning residual model parameters within a specified range. The output is a horizon-based semblance plot for a layer where the maximum amplitudes indicate the best-fit model perturbations.

The raypaths and tomographic coefficients are computed in the background medium for sparse lateral locations and for different offsets. For each series of offsets, a given horizon is considered a reflection surface. The upper horizons are considered transmission surfaces, as shown in Figure 1a. The tilted reflectors are tangent to the hori-

zons. Horizontal lines show the vertical locations of the reflection/transmission points in the locally 1D model.

In the RMO equations 35–37, the traveltime error is divided into the contributions of the updated overburden model and the current layer parameter (layer N). Only one of the residuals $\{\Delta V_N, \Delta\delta_N, \Delta\varepsilon_N\}$ is scanned each time. The interval velocities (or δ) are updated using short-offset reflection events ($\leq 30°$); ε is updated using long-offset data. Steep dips in the model contribute considerably to the RMOs' sensitivity to changes in ε.

This approach suffers from the general limitations of layer-stripping methods. Inaccuracies in overburden-parameter estimation affect the parameters of the current layer (Figure 1b).

SYNTHETIC EXAMPLE

Figures 2–8 present the local tomography method through a simple synthetic example. The left subplot of Figure 2 shows the velocity section. The vertical axis of the section is depth in meters. The vertical profile of the true VTI parameters — interval velocity, δ, and ε, with the corresponding synthetic gather (calculated by anisotropic ray tracing) — are shown in the center subplot. The right subplot of Figure 2 shows the CMP gather for trace 101. In this schematic example, the velocity and δ are considered to be known and accurate, and the goal is to update ε after an error has been introduced in each layer. Anisotropic curved-ray time migration is performed for the incorrect ε model parameters.

Figure 3 shows the ε analysis in the first layer. The migrated gather for the selected location and the nonflattened event related to the first layer are shown in the right-hand panels of Figure 3a. Starting from the initial estimate $\varepsilon = 0.125$, we obtain $\varepsilon = 0.175$ (see maximum value of the histogram related to the optimum residual ε); the exact value is $\varepsilon = 0.2$. The lower-left subplot in Figure 3a shows the background velocity, the background δ, and the background ε of the first layer. The lower central subplot in Figure 3a shows the semblance (percent, horizontal axis) versus residual ε (vertical axis). The lower-right subplot is a zoom of the upper-right subplot (time-migrated gather). In Figure 3b, the background, residual, and updated values of ε are shown along both the vertical axis and the horizontal extension of the first layer. The corresponding flattened event is shown in the Corrected panel.

Figure 4 shows the residual ε analysis in the second layer, after the residual ε values for the first layer have been picked. Starting at $\varepsilon = 0.1$, we obtain $\varepsilon = 0.125$ (see histogram); the true value is $\varepsilon = 0.15$. The resulting RMO includes contributions of traveltime errors from two layers — the overburden layer and the current layer.

Figure 5 shows the residual ε analysis in the third layer, where the residuals for the first and the second layers have been picked. Starting at $\varepsilon = 0.125$, we obtain $\varepsilon = 0.185$ (see histogram); the true value is $\varepsilon = 0.2$. The resulting RMO includes contributions of traveltime errors from the two overburden layers and from the current layer. The background ε field was updated with the residual values, and a new anisotropic migration was performed. An additional iteration was applied, which resulted in almost perfect values. Figures 6–8 show the second iteration.

REAL DATA EXAMPLE

Figures 9–12 demonstrate a seismic line in offshore Texas, where a local laterally invariant 1D VTI medium is assumed. In this example, we used CIGs at every twentieth common-reflection-point

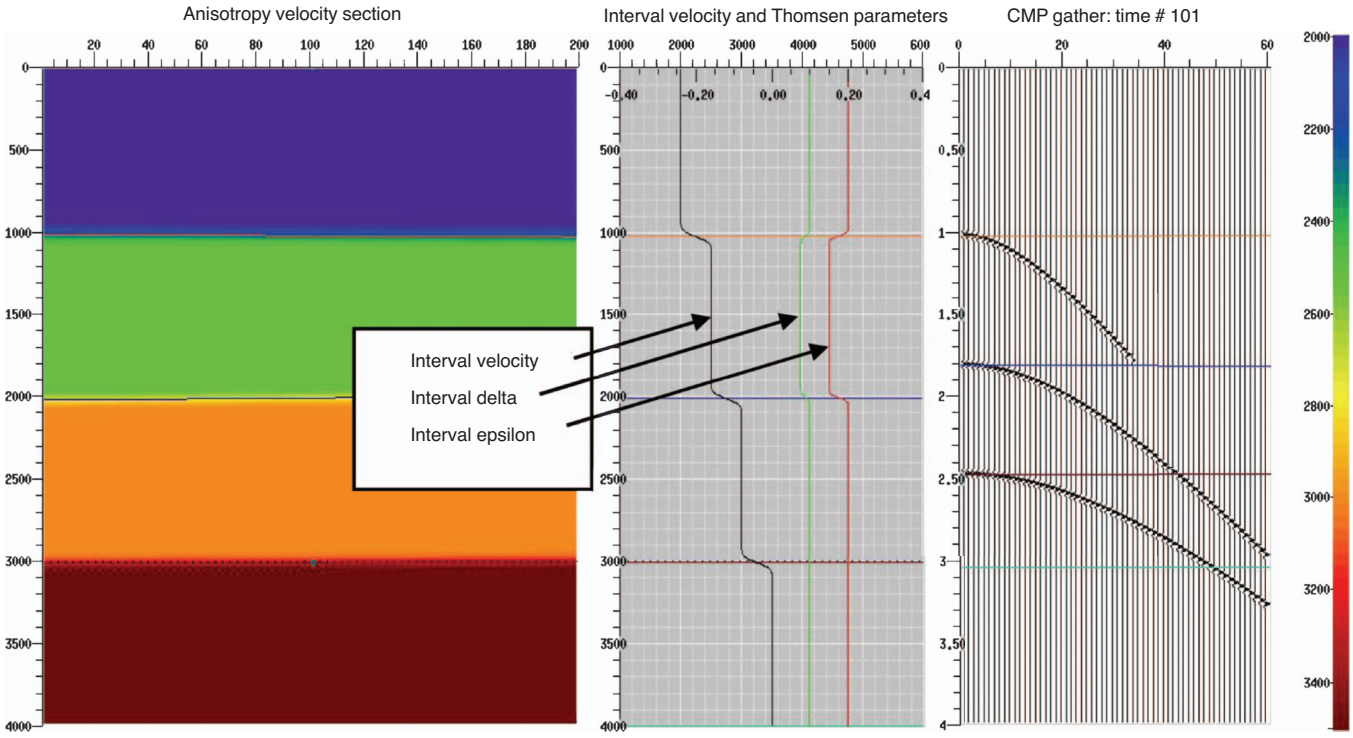

Figure 2. Synthetic anisotropic model. The units of the horizontal axis are common-midpoint (CMP) numbers, and the lateral distance between two successive traces is 100 m. The colors in the section correspond to the color bar on the right, graded in meters per second. The vertical axis of the center subplot is depth in meters. The units of labels on the horizontal axis are meters per second for velocity and dimensionless for Thomsen parameters.

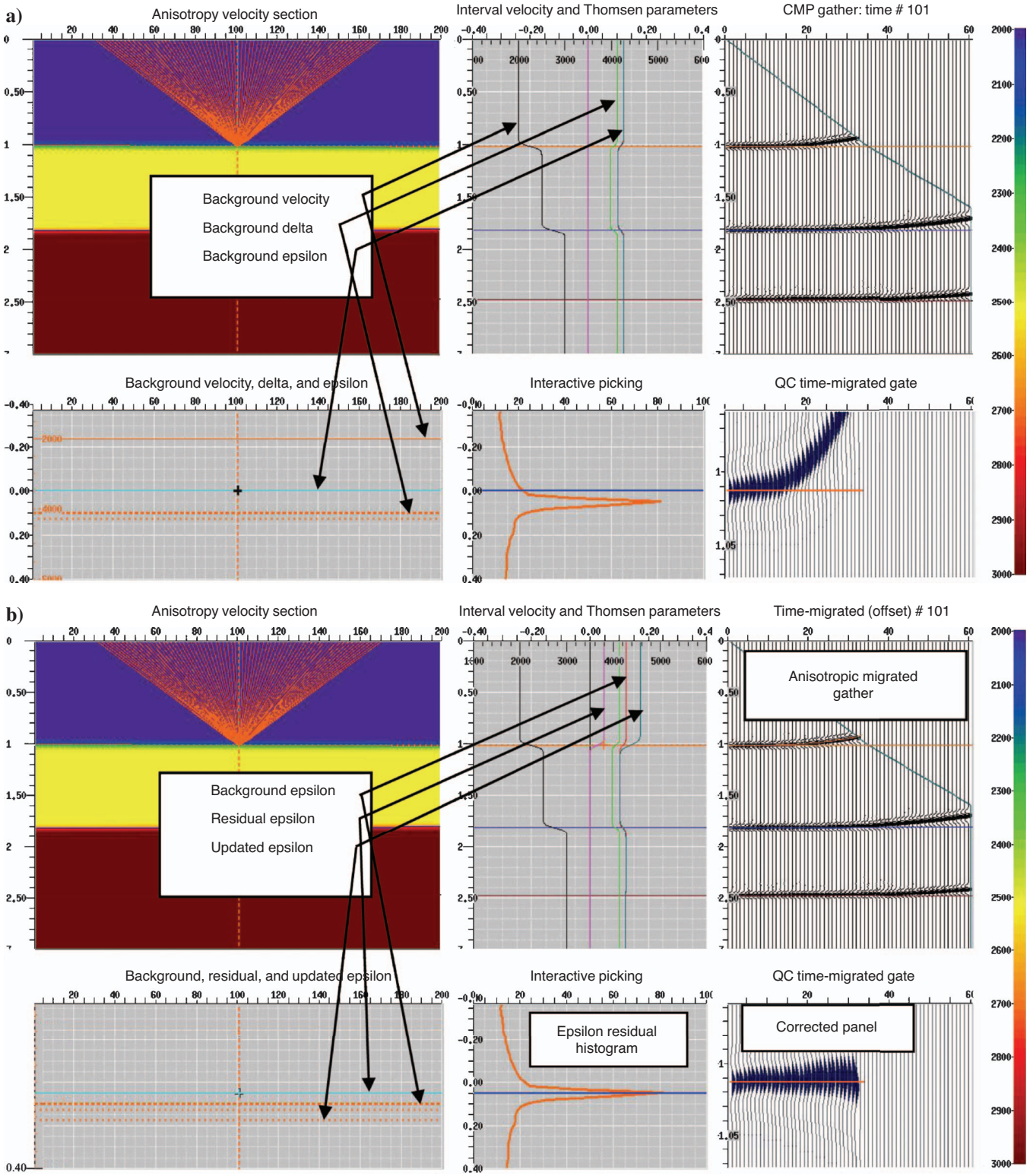

Figure 3. The ε correction at the first layer. True value 0.2, background value 0.125, residual 0.05, updated value 0.175: (a) before updating, (b) after updating. The vertical axis of the three upper subplots in Figure 3a is vertical time in seconds. The units of the vertical axis in the lower-left portion of (a) are meters per second for velocity and dimensionless for Thomsen parameters.

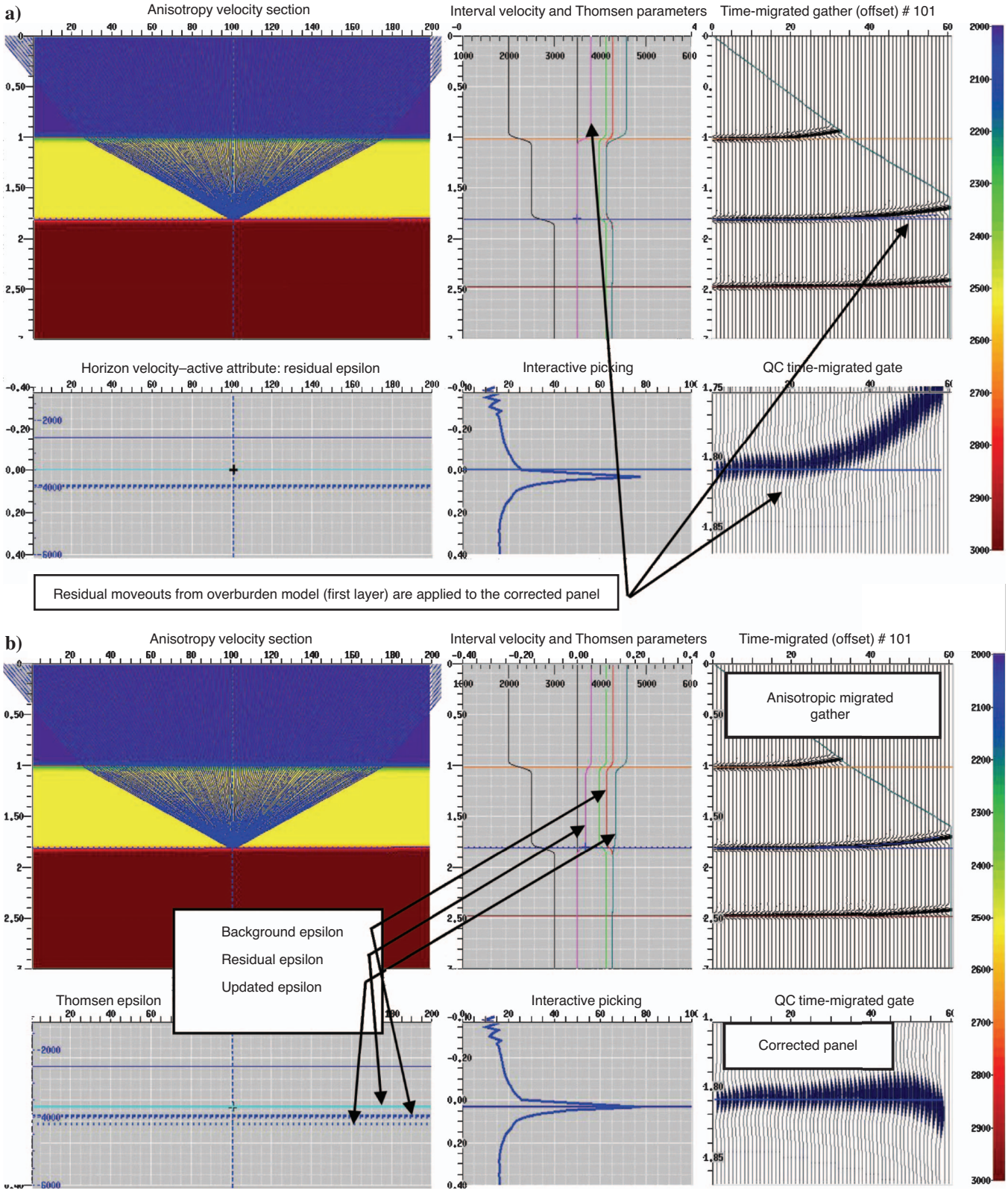

Figure 4. The ε correction at the second layer. True value 0.15, background value 0.1, residual 0.025, updated value 0.125: (a) before updating, (b) after updating.

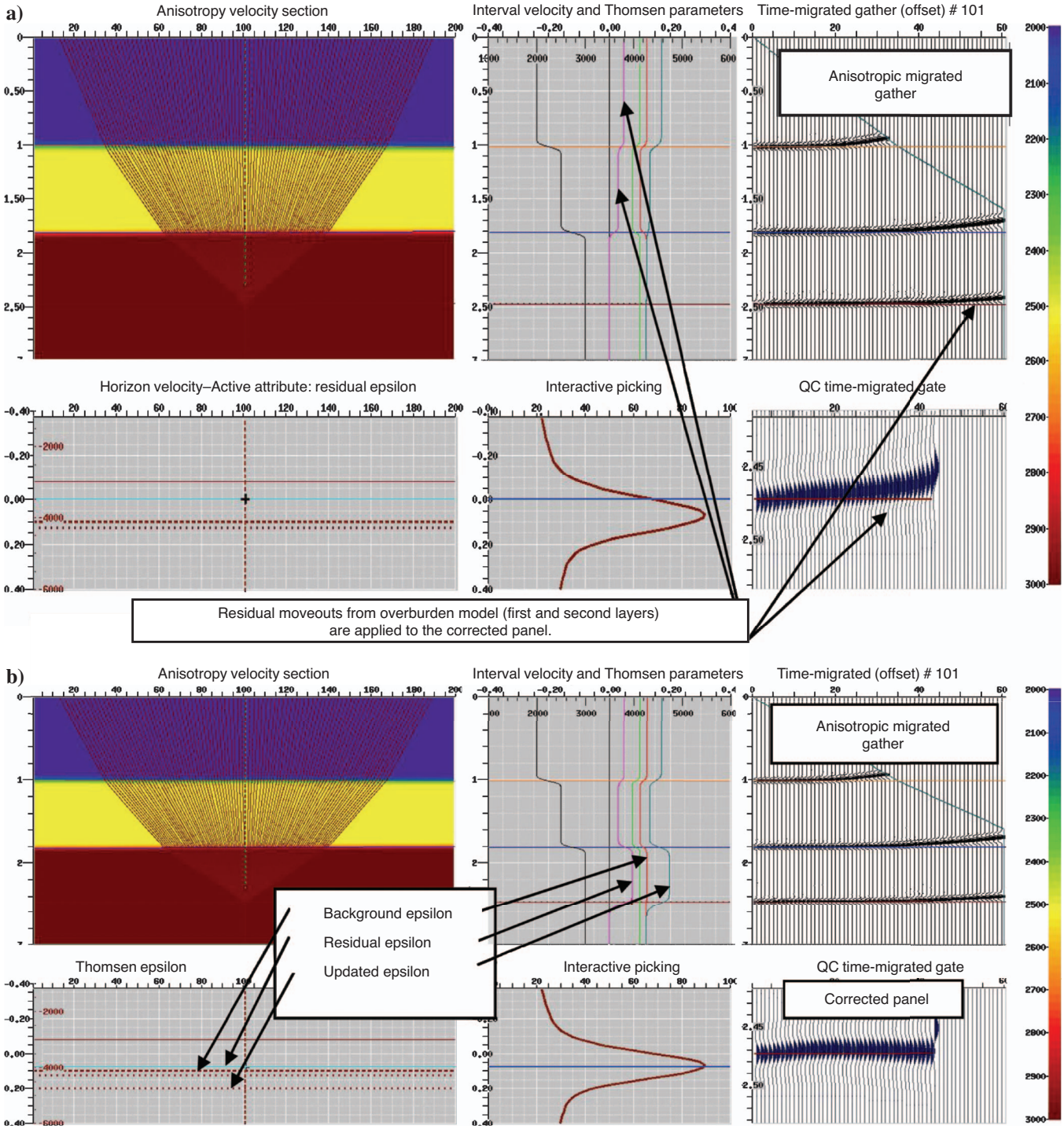

Figure 5. The ε correction at the third layer. True value 0.2, background value 0.125, residual 0.06, updated value 0.185: (a) before updating, (b) after updating.

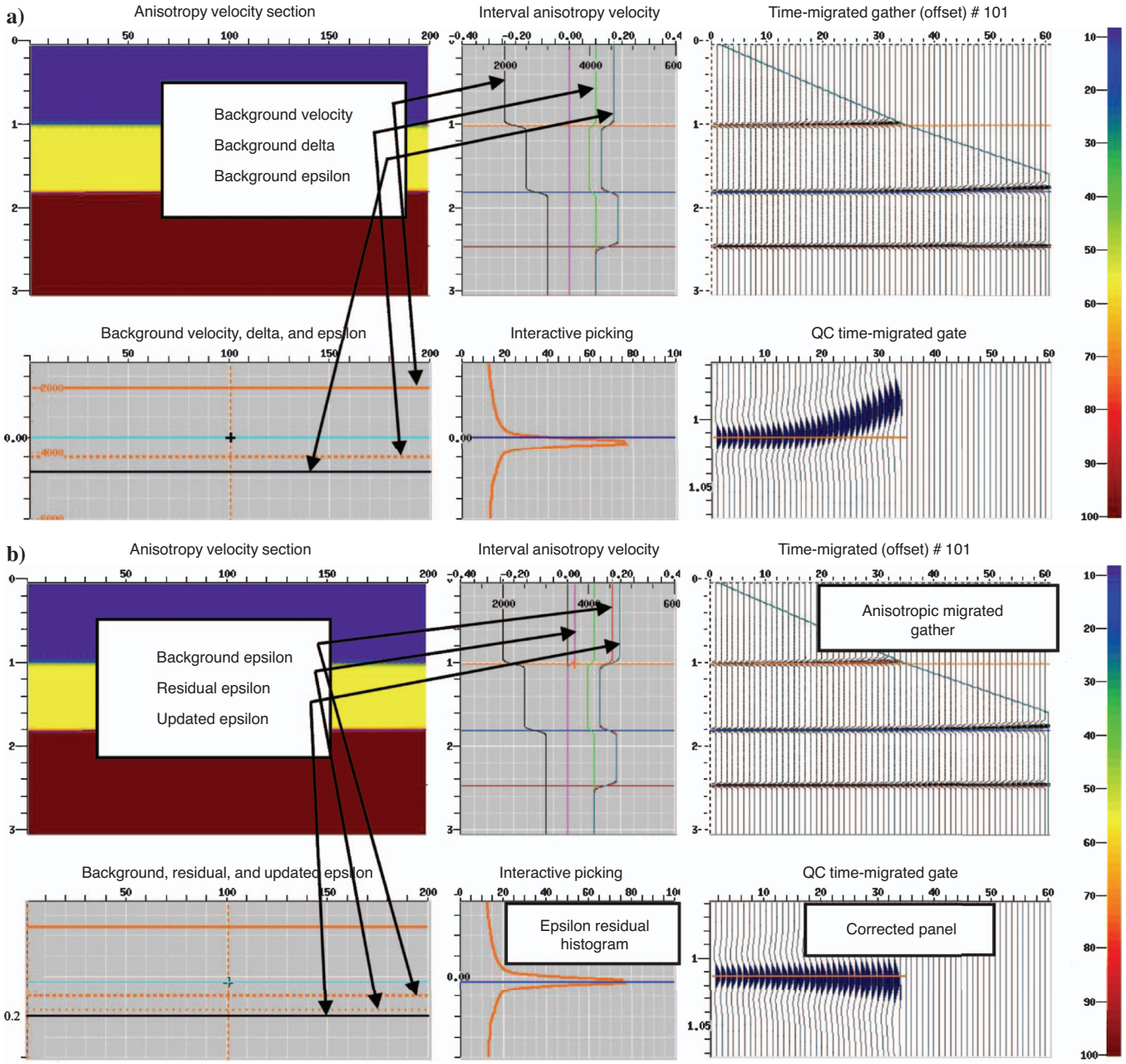

Figure 6. Second iteration, ε correction at the first layer. True value 0.2, background value 0.175, residual 0.024, updated value 0.199: (a) before updating, (b) after updating.

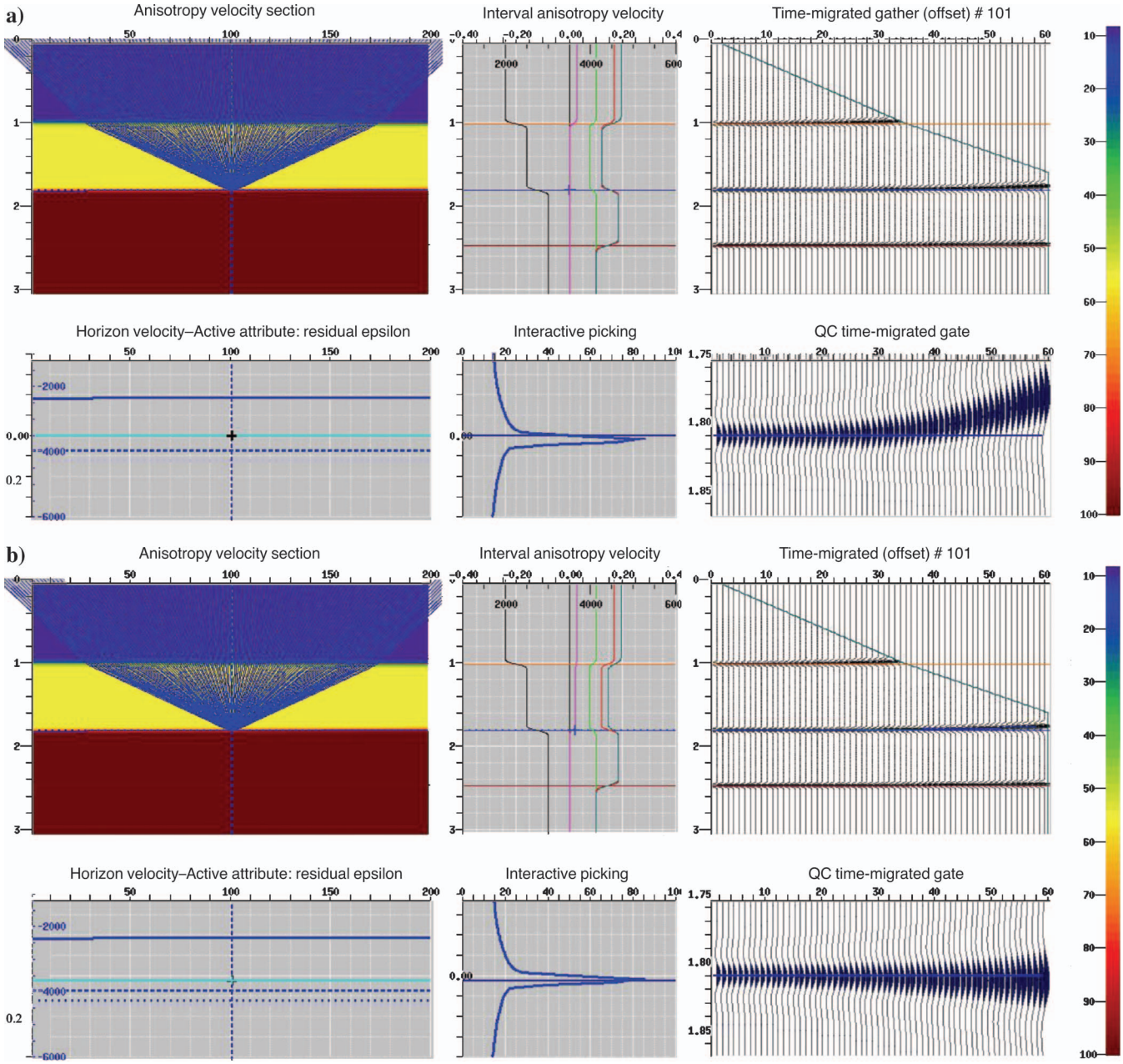

Figure 7. Second iteration, ε correction at the second layer. True value 0.15, background value 0.125, residual 0.022, updated value 0.147: (a) before updating, (b) after updating.

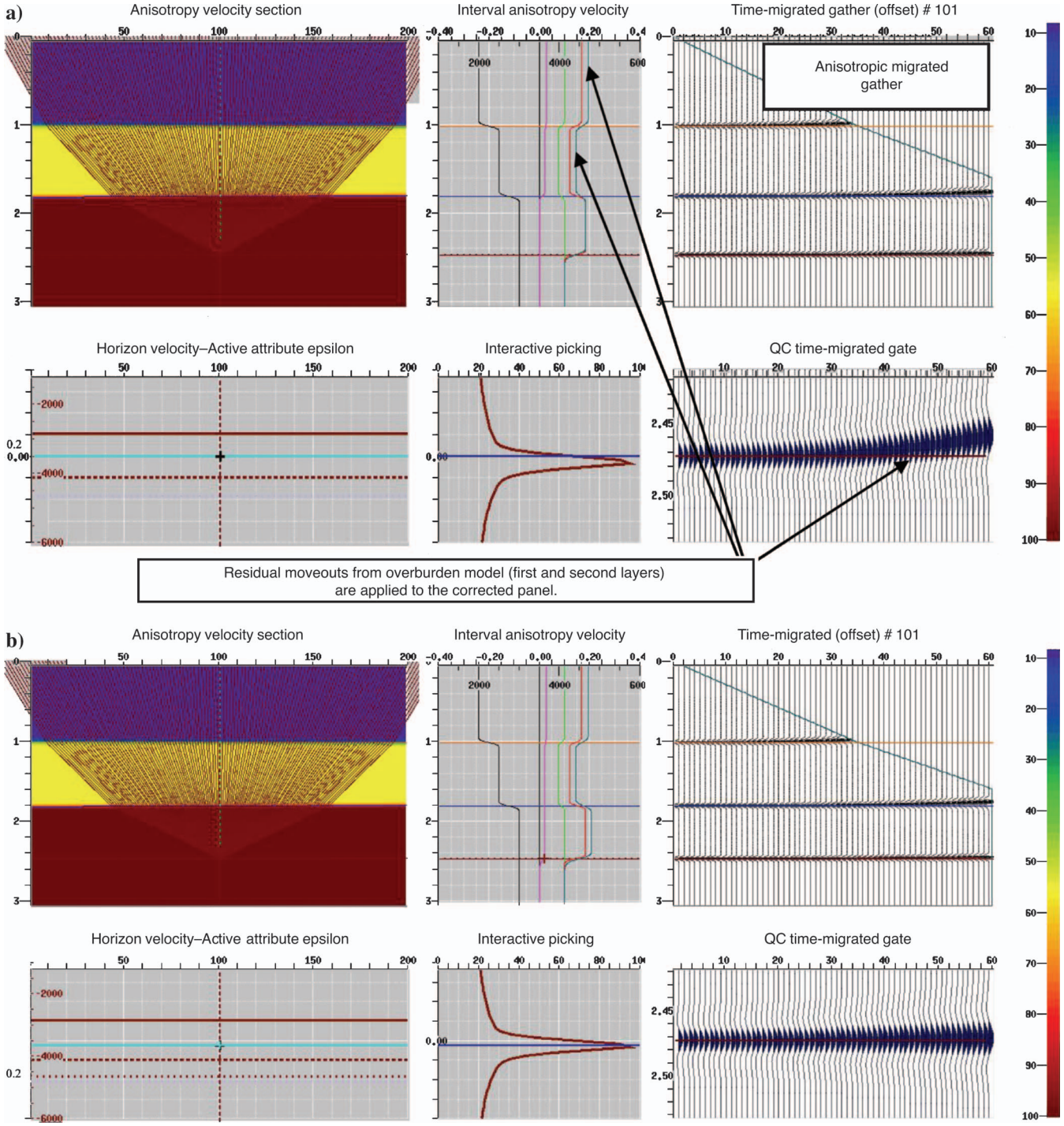

Figure 8. Second iteration, ε correction at the third layer. True value 0.2, background value 0.185, residual 0.017, updated value 0.202: (a) before updating, (b) after updating.

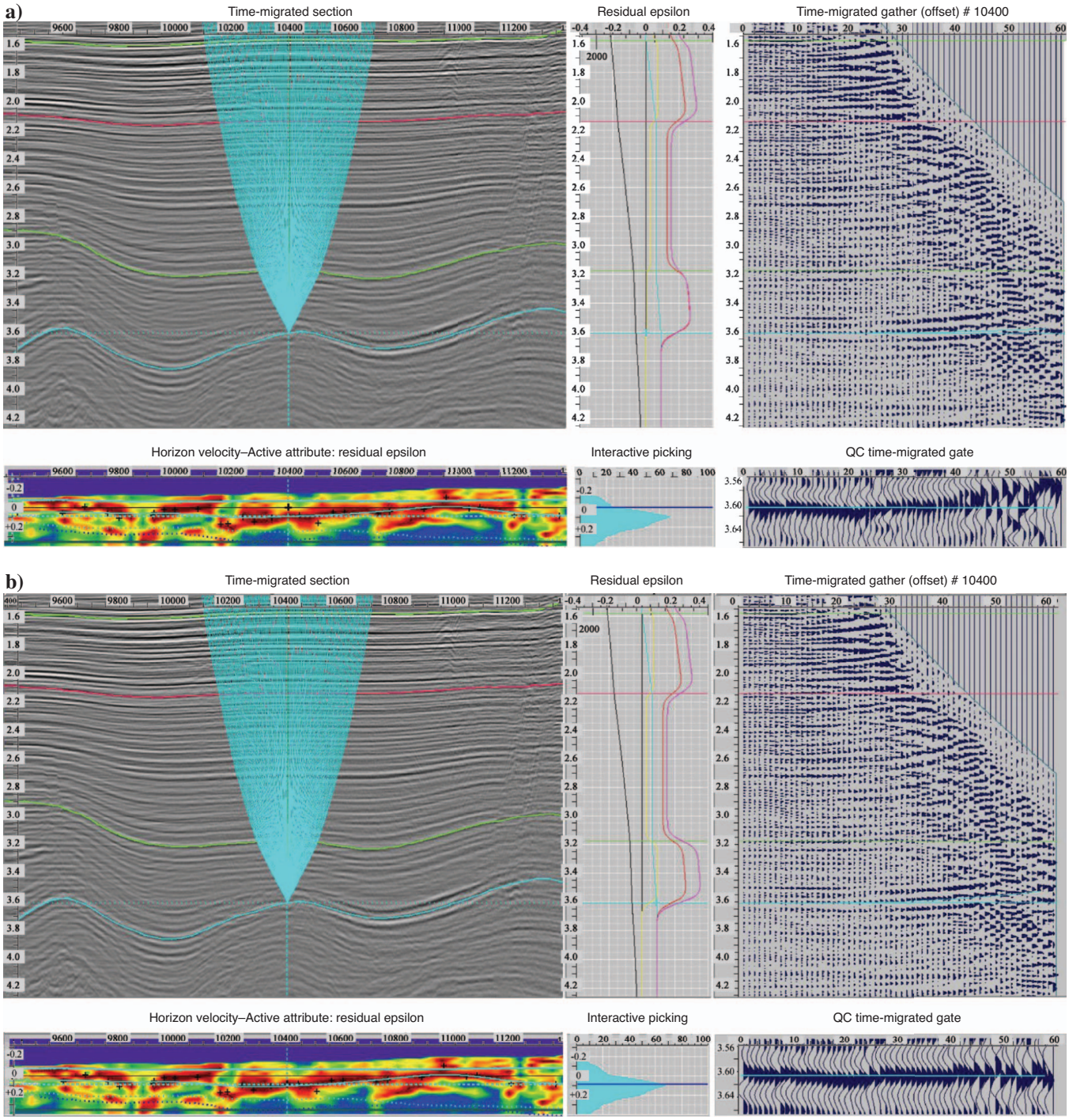

Figure 9. Residual ε analysis for layer 5. Background value varies linearly in vertical time: $\varepsilon = 0.24$ at the upper interface of the layer (horizon 4) and $\varepsilon = 0.27$ at the lower interface of the layer. The maximum values on the semblance plot (lower-left panel) correspond to the optimum residual ε. (a) Before residual picking. (b) After residual picking. The maximum coherency corresponds to residual $\Delta\varepsilon = 0.08$. In the upper central panel of (a) velocity on the horizontal axis is in meters per second; the dimensionless labels correspond to Thomsen parameters. The black line shows the background velocity; the yellow line, background δ; the red line, background ε; the turquoise line, residual ε; and the pink line, updated ε.

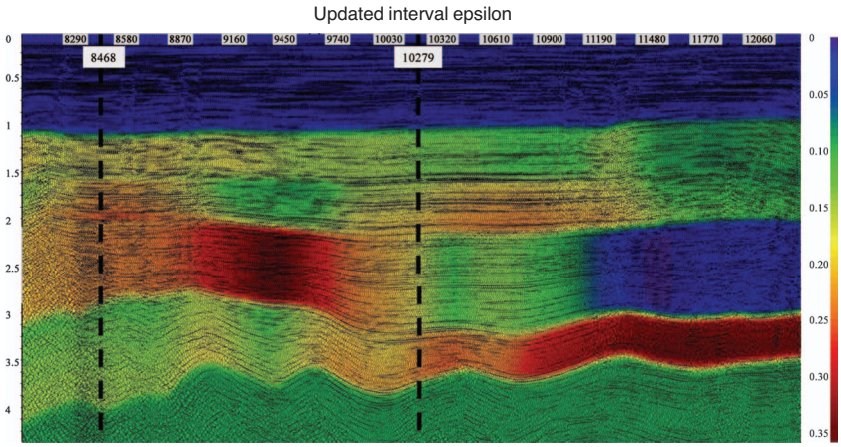

Figure 10. Time-migrated section with final ε values overlain. Blue corresponds to $\varepsilon = 0$; red corresponds to $\varepsilon_{max} = 0.35$. Horizontal axis shows CRP numbers. Vertical time is in seconds. Vertical dashed lines indicate CRP locations of the image gathers shown in Figure 11.

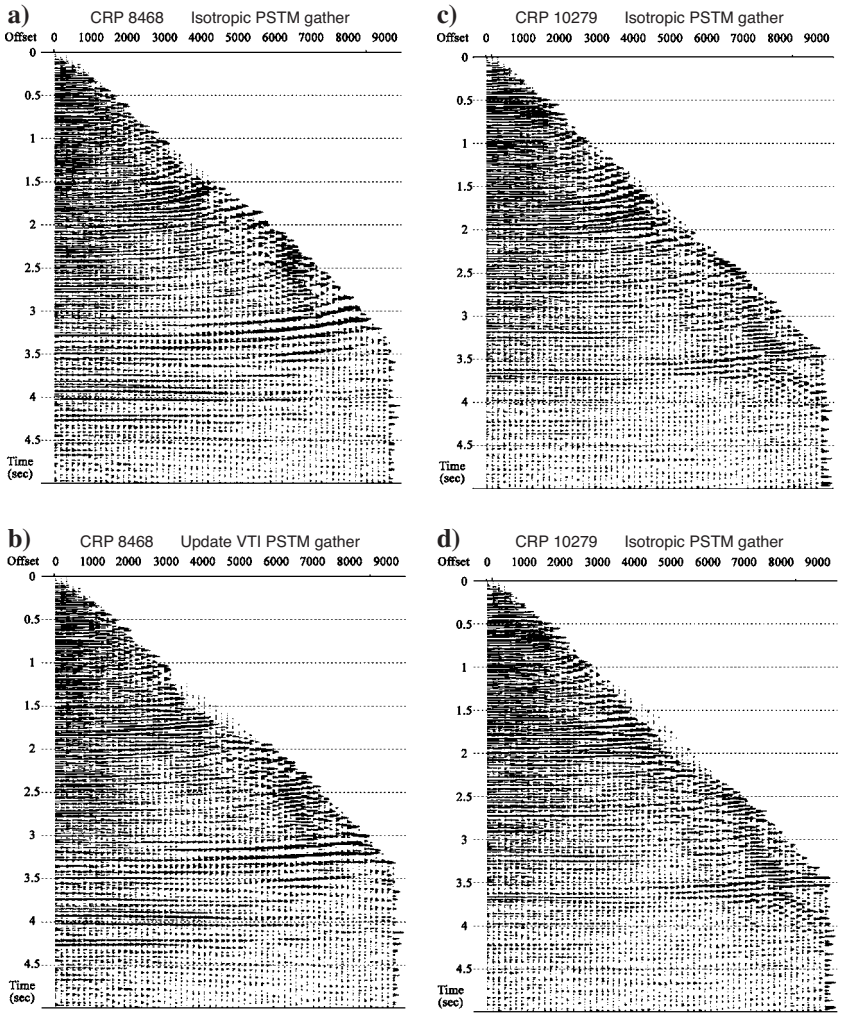

Figure 11. Image gathers generated by curved-ray Kirchhoff time migration. Horizontal axis shows offset in meters; vertical time is in seconds along the vertical axes. (a, b) Before and after updating at CRP 8468. (c, d) Before and after updating at CRP 10279.

(CRP) location to update ε. The background parameters are instantaneous (interval) vertical compression velocity and Thomsen anisotropy parameters δ and ε. In this example, δ values assigned to horizons were computed from wells located in the area. Through the layers (between the interface horizons), δ and ε were assumed linearly varying in vertical time. Initially, we set $\varepsilon = \delta$ for all layers and performed anisotropic curved-ray Kirchhoff time migration. The objective was to update ε by applying local tomography. The method was applied layer by layer from the top down using time-migrated gathers with a maximum offset of 9 km (about 30,000 feet). The hockey-stick curves associated with the error in ε are seen clearly on the far-offset migrated gather events.

Figure 9 shows the residual ε analysis for layer five, before and after ε updating. On the time-migrated section panel, the horizontal axis shows the CRP index; the vertical axis is vertical time in seconds. The units of offset on the time-migrated gather panel (horizontal axis) are CRP traces. The upper central subplot in Figure 9a shows the medium properties versus vertical time in seconds. For the four layers above, residual ε values have been estimated. The background value for layer five varies linearly in the range of $0.24 \leq \varepsilon \leq 0.27$, and the residual value found at the selected lateral location (CRP 10400) is 0.08.

Figure 10 shows the time-migrated section with the updated ε values overlain; the CRP index lies along the horizontal axis, and the vertical time is in seconds along the vertical axis. The color scale corresponds to different values of parameter ε — blue corresponds to $\varepsilon = 0$, and red to $\varepsilon_{max} = 0.35$. Two lateral locations, shown by dashed lines, compare the migrated gathers before and after the ε updating (see Figure 11). The two upper plots show the migrated gathers before and after updating at CRP 8468, and the two lower plots at CRP 10279. An improved flattening of the events is visible after updating. However, the approach does not intend to flatten gathers fully, and it does not pretend to find an optimal updated model. It primarily aims to find the long-wavelength residual parameters to build a background initial model, to be further updated by a global tomographic approach.

Figure 12 shows the time-migrated images at two different locations, with the CRP index along the horizontal axes and the vertical time in milliseconds along the vertical axes. The left-hand plots represent the migrated images before ε updating, and the right-hand plots represent after ε updating. The right-hand panel shows that imaging with updated ε improves continuity, enhances amplitude, and enables better fault imaging.

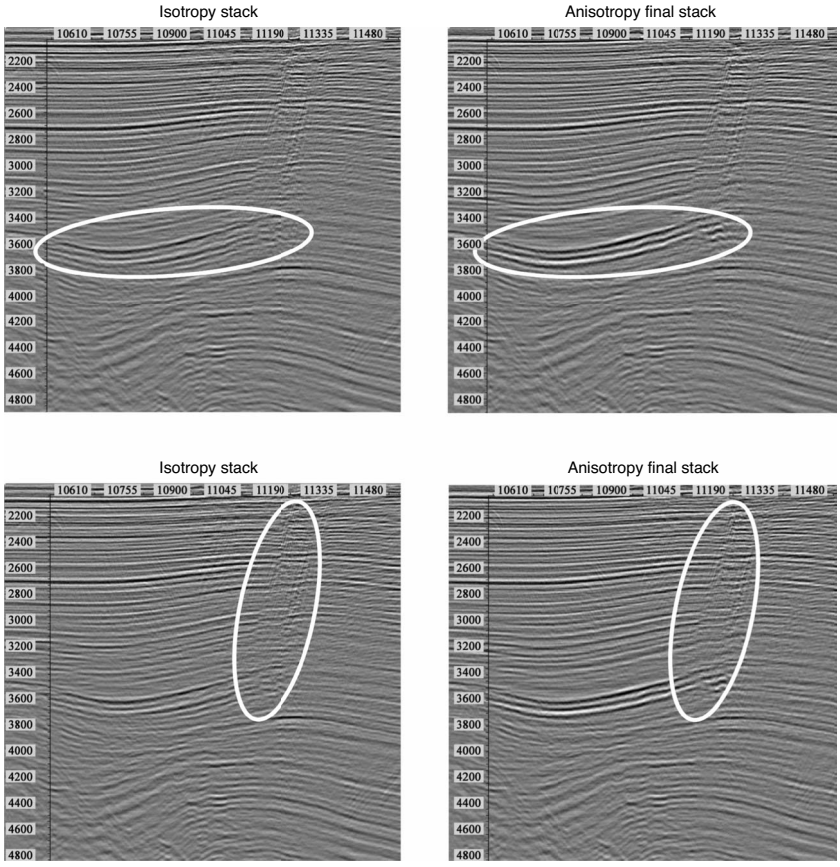

Figure 12. Time-migrated images at two different locations (upper and lower plots) before (left) and after (right) ε updating. The improvements in continuity, the enhanced amplitude, and better fault imaging are clearly seen. Horizontal axis shows CRP numbers. Vertical time is in milliseconds.

CONCLUSIONS

This paper describes a new local tomography method for updating background anisotropic velocity parameters in a controlled manner. The method is applied as an interactive residual-interval-parameter analysis and operates directly on image gathers. Dividing the contribution to the computed RMO into two components — that of the overburden residual parameters and that of the analyzed interval — makes it possible to perform direct residual-interval-parameter analysis in the same way that residual-effective-parameter analysis is performed. Local tomography enables a controlled interactive estimation of long-wavelength anisotropy parameters. The reliable anisotropy parameters estimated by the local approach can be used as a background (guiding) model to improve the convergence of global tomography, where inversion is performed simultaneously for all parameters, using detailed RMO information.

ACKNOWLEDGMENTS

We are grateful to Paradigm for its financial and technical support of this study. We thank Vladimir Grechka for numerous helpful discussions about the range of anisotropic parameters. Gratitude is extended to the editors and reviewers, whose valuable suggestions and comments helped improve the content and style of this paper.

APPENDIX A

BOUNDARY-VALUE RAY TRACING WITH TILTED REFLECTOR

The given data are the vertical time and orientation of the reflection surface specified at the reflection point and the offset length and azimuth that refer to the earth's surface. Background-medium properties versus vertical time are known. The curved raypath is presented in Figure A-1. Points S and R are source and receiver locations on the earth's surface, associated with a given reflection event; I is the image point; U is the projection of the image point on the earth's surface; and N is the intersection of the normal line to the reflection surface (that passes through the image point I) with the earth's surface. Note that the length (offset) and direction (azimuth) of vector $\overrightarrow{SR}$ are specified, not the specific locations of S and R.

In the case of a tilted normal to the reflection surface (dipping reflector), the planes of incident and reflected paths are different. The curved path IS of the incident ray is in the vertical plane ISU, and the curved path of the reflected ray is in another vertical plane IRU. The azimuths of these two vertical planes are different. At the reflection point I, the phase velocity of the incident ray $V^{\text{in}}_{\text{phs}}$, the phase velocity of the reflected ray $V^{\text{re}}_{\text{phs}}$, and the normal IN to the reflection surface are in the same (generally nonvertical) plane SIR. The inward normal IN to the reflection surface is defined by the dip angle α and azimuth φ. The source-receiver offset SR in the horizontal plane is described by its absolute value H and azimuth β.

Let d_S and d_R be lateral shifts of the incident and reflected rays, respectively. They depend on the corresponding horizontal slownesses p^{in}_h and p^{re}_h. These shifts result from the initial-value ray tracing and can be computed numerically:

$$d_S = d_S(p^{\text{in}}_h), \quad d_R = d_R(p^{\text{re}}_h). \tag{A-1}$$

The (horizontal) surface shifts d_S and d_R are functions of the unknown ray parameters p^{in}_h and p^{re}_h, respectively. The offset vector $\overrightarrow{SR} = \overrightarrow{UR} - \overrightarrow{US}$ can be decomposed into two horizontal components, H_x and H_y:

$$\begin{aligned} d_R(p^{\text{re}}_h) \cdot \cos\varphi_R - d_S(p^{\text{in}}_h) \cdot \cos\varphi_S &= H\cos\beta \equiv H_x, \\ d_R(p^{\text{re}}_h) \cdot \sin\varphi_R - d_S(p^{\text{re}}_h) \cdot \sin\varphi_S &= H\sin\beta \equiv H_y, \end{aligned} \tag{A-2}$$

where φ_S and φ_R are azimuth angles of shifts d_S and d_R, respectively (see Figure A-2). If the symmetry axis of the medium is vertical and the medium properties are functions of depth only, then the entire paths of the incident and reflected rays lie in the vertical planes of azimuths φ_S and φ_R, respectively. Equation set A-2 is solved for the azimuths of the incident and reflected paths. The azimuths φ_S and φ_R are functions of the lateral shifts d_S and d_R, which are functions of the ray parameters p_h^{in} and p_h^{re}.

Let vector $\mathbf{n}$ be an inward normal to the reflection surface. Assume, for the sake of symmetry, that both arrays, the incident and the reflected, arrive at the reflection point. Then for a general anisotropic medium, Snell's reflection law is

$$(\mathbf{p}^{\text{in}} + \mathbf{p}^{\text{re}}) \times \mathbf{n} = 0. \tag{A-3}$$

Vector equation A-3 leads to three scalar equations, but only two of them are independent. Discard the z-component of the cross product and introduce the azimuths φ_S and φ_R to get

$$\begin{aligned}(p_h^{\text{in}} \cos\varphi_S + p_h^{\text{re}} \cos\varphi_R)n_z &= (p_z^{\text{in}} + p_z^{\text{re}})n_x,\\ (p_h^{\text{in}} \sin\varphi_S + p_h^{\text{re}} \sin\varphi_R)n_z &= (p_z^{\text{in}} + p_z^{\text{re}})n_y.\end{aligned} \tag{A-4}$$

Note that the vertical-slowness components at the reflection point, p_z^{in} and p_z^{re}, are not independent values. They are defined (up to the sign) by the corresponding horizontal slowness and also depend on the medium properties at the reflection point. The dependency $p_z(p_h)$ follows from the Christoffel equation for the VTI medium. Recall

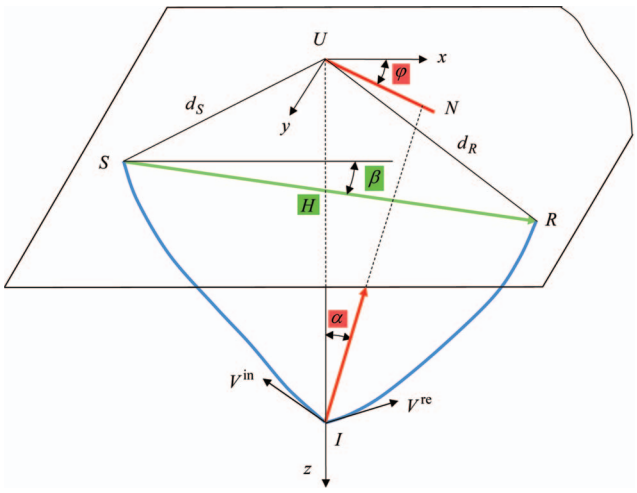

Figure A-1. Boundary value ray-tracing scheme.

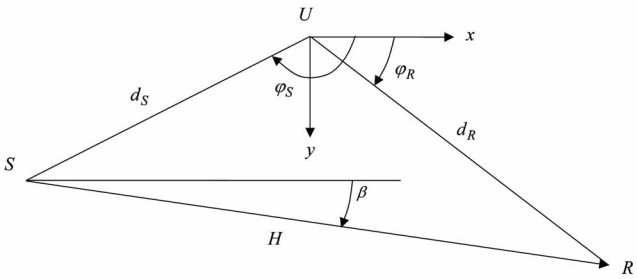

Figure A-2. Horizontal shifts of the incident and reflected rays. Top view is from the earth's surface.

that the azimuths φ_S and φ_R are also defined by the horizontal slowness (equation set A-2). Thus, equation set A-4 includes only two independent parameters, p_h^{in} and p_h^{re}, and can be solved numerically.

For a horizontal reflector, the normal to the reflection surface becomes vertical and coincides with the medium axis of symmetry. The incident and reflected paths become identical, with their lateral shifts equal and azimuths opposite:

$$d_S = d_R = \frac{H}{2}, \quad \varphi_R = \beta, \quad \varphi_S = \beta + \pi, \tag{A-5}$$

where H is the offset magnitude and β is the offset azimuth. For a flat (horizontal) reflector, one may accept $\beta = 0$ without any loss of generality. The ray parameters p_h^{in} and p_h^{re} are equal, and they are defined by solving the nonlinear equation numerically:

$$h(p_h) = \frac{H}{2}, \tag{A-6}$$

where the lateral shift h on the earth's surface is the result of ray tracing.

APPENDIX B

RESIDUAL TRAVELTIME FOR UPDATED MEDIUM

Perturbations of VTI properties affect residual traveltime. The perturbed parameters of the medium are vertical velocity V_{P} and Thomsen parameters δ and ε. Perturbations are assumed to be small, and the response of the medium is linearized. It follows from equation 17 that the variation of traveltime on the infinitesimal raypath interval is

$$\begin{aligned}\frac{\Delta(dt)}{d\sigma} = \frac{\partial G}{\partial p_h}\cdot\Delta p_h + \frac{\partial G}{\partial p_z}\cdot\Delta p_z + \Delta\left(\frac{\partial G}{\partial p_h}\right)\cdot p_h\\ + \Delta\left(\frac{\partial G}{\partial p_z}\right)\cdot p_z.\end{aligned} \tag{B-1}$$

Taking into account the ray-tracing equation set 6, this variation can be presented as

$$\begin{aligned}\frac{\Delta(dt)}{d\sigma} = \frac{\partial G}{\partial p_h}\cdot\Delta p_h + \frac{\partial G}{\partial p_z}\cdot\Delta p_z + \frac{\Delta(dh)}{d\sigma}\cdot p_h\\ + \frac{\Delta(dz)}{d\sigma}\cdot p_z.\end{aligned} \tag{B-2}$$

According to a basic tomographic assumption, the ray trajectory is considered stationary. The effect of raypath change (from small perturbations of the medium properties) on the traveltime is assumed negligible. Therefore, the traveltime variation on the infinitesimal interval of the ray trajectory $\Delta(dt)$ can be simplified to

$$\frac{\Delta(dt)}{d\sigma} = \frac{\partial G}{\partial p_h}\cdot\Delta p_h + \frac{\partial G}{\partial p_z}\cdot\Delta p_z. \tag{B-3}$$

Integration yields the residual traveltime along the entire raypath:

$$\Delta t^{\text{medium}} = \sum_{k=1}^{N}\int_{\sigma_k}\left(\Delta p_h\cdot\frac{\partial G}{\partial p_h} + \Delta p_z\cdot\frac{\partial G}{\partial p_z}\right)d\sigma, \tag{B-4}$$

where k is the layer index. The superscript *medium* indicates that traveltime variation is caused by updating the medium properties only.

Recall that the Hamiltonian vanishes along the ray and its variation is identically zero. Therefore,

$$\frac{\partial G}{\partial p_h}\Delta p_h + \frac{\partial G}{\partial p_z}\Delta p_z = -\left(\frac{\partial G}{\partial V_{\mathrm{P}}}\Delta V_{\mathrm{P}} + \frac{\partial G}{\partial \delta}\Delta\delta + \frac{\partial G}{\partial \varepsilon}\Delta\varepsilon\right). \tag{B-5}$$

Combine equations B-4 and B-5, and recall that residuals of the medium properties ΔV_k, $\Delta\varepsilon_k$, and $\Delta\delta_k$ are assumed constant through a fixed layer k. The one-way residual time equation becomes

$$\Delta t^{\mathrm{medium}} = -\sum_{k=1}^{N}\left(\Delta V_k \cdot \int_{\sigma_k}\frac{\partial G}{\partial V}d\sigma + \Delta\delta_k \cdot \int_{\sigma_k}\frac{\partial G}{\partial \delta}d\sigma + \Delta\varepsilon_k \cdot \int_{\sigma_k}\frac{\partial G}{\partial \varepsilon}d\sigma\right). \tag{B-6}$$

APPENDIX C

RESIDUAL TRAVELTIME FROM HORIZON SHIFTS

The two-way raypath with geologic formations separated by horizon interfaces is shown schematically in Figure C-1. We consider the traveltime residual caused by the shift of the reflection point. A similar relationship holds for the traveltime residual caused by the shifts of the transmission points. The shift of the reflection point is shown schematically in Figure C-2a.

We introduce the notation for the sum of slowness of the two rays, incident and reflected (for symmetry, both rays are assumed arriving to the image point), as

$$\mathbf{p}^{\mathrm{horizon}} \equiv \mathbf{p}^{\mathrm{in}} + \mathbf{p}^{\mathrm{re}}. \tag{C-1}$$

It follows from Snell's law that a small shift of the image point along the reflection horizon does not affect the total incident-reflected traveltime. The residual traveltime caused by the horizon shift can be presented as

$$\Delta t^{\mathrm{horizon\ shift}} = \mathbf{p}^{\mathrm{horizon}} \cdot \Delta\mathbf{d}. \tag{C-2}$$

Furthermore, the horizon shift vector $\Delta\mathbf{d}$ can be decomposed into two components: normal to the horizon surface and tangent to this surface. The tangent shift has no meaning for tomography; therefore, we can assume the horizon shift has only a normal component:

$$\Delta\mathbf{d} = \Delta d\mathbf{n}, \tag{C-3}$$

where Δd is a scalar value and $\mathbf{n}$ is the normal direction vector (of unit length). Combining equations C-2 and C-3 results in

$$\frac{\partial t^{\mathrm{horizon\ shift}}}{\partial d} = \mathbf{p}^{\mathrm{horizon}} \cdot \mathbf{n} = (\mathbf{p}^{\mathrm{in}} + \mathbf{p}^{\mathrm{re}}) \cdot \mathbf{n}. \tag{C-4}$$

The tomographic coefficient of the horizon shift is a scalar product of normal direction and the sum of ray pair slowness. For the inward normal, both rays should arrive at the image point. Alternatively, the two rays can emerge from the image point, but in this case the normal should face outward.

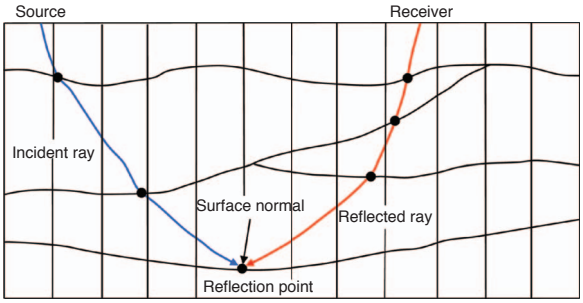

Figure C-1. Schematic representation of two-way raypath with reflection and transmission points on geological horizons.

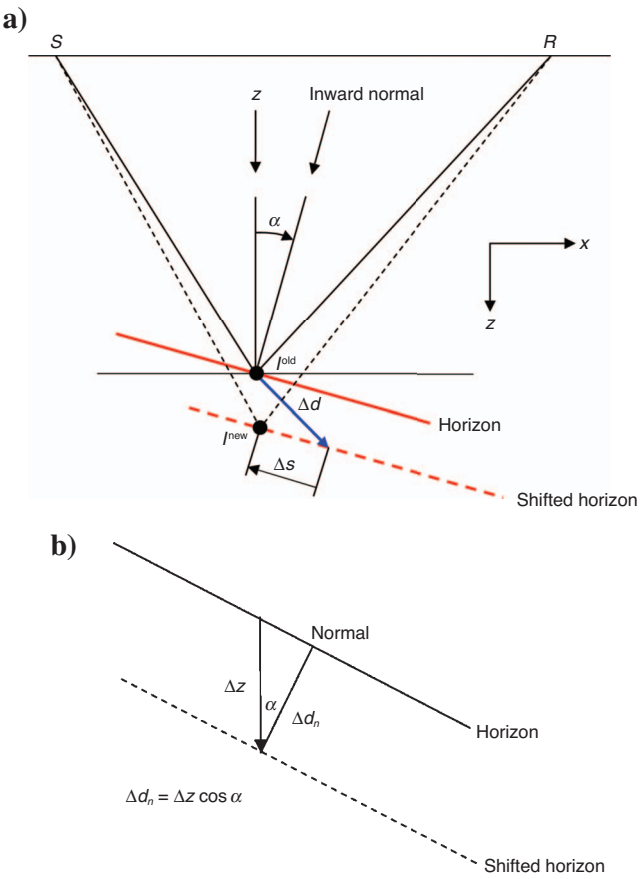

Figure C-2. (a) Schematic representation of the reflection point shift. (b) Replacement of normal horizon shift by vertical shift.

Consider a particular case where the horizon shift is vertical. With no loss of generality, any shift of a planar (or locally planar) horizon can be presented by a vertical shift:

$$\Delta d_x = 0, \quad \Delta d_y = 0, \quad \Delta d_z = \Delta z. \tag{C-5}$$

Replacement of the normal shift by the vertical shift is shown in Figure C-2b. The normal shift is

$$\Delta d_n = \Delta z \cos \alpha = \Delta z n_z. \tag{C-6}$$

Combining equations C-2 and C-6 and taking into account Snell's law, we obtain,

$$A_z^{\text{horizon}} = \frac{\Delta t^{\text{horizon shift}}}{\Delta z} = p_z^{\text{horizon}}, \tag{C-7}$$

where p_z^{horizon} is defined according to equation C-2. For the two rays considered departing from the reflection point, we negate the sign in equation C-7:

$$\underbrace{A_z^{\text{horizon}} = +\, p_z^{\text{horizon}}}_{\text{for rays arriving to reflection point}}, \quad \underbrace{A_z^{\text{horizon}} = -\, p_z^{\text{horizon}}}_{\text{for rays departing from reflection point}}. \tag{C-8}$$

REFERENCES

Alkhalifah, T., 1997a, Seismic data processing in vertically inhomogeneous TI media: Geophysics, **62**, 662–675.

——– 1997b, Velocity analysis using nonhyperbolic moveout in transversely isotropic media: Geophysics, **62**, 1839–1854.

Bishop, T. N., K. P. Bube, R. T. Cutler, R. T. Langan, P. L. Love, J. R. Resnick, R. T. Shuey, D. A. Spindler, and H. W. Wyld, 1985, Tomographic determination of velocity and depth in laterally varying media: Geophysics, **50**, 903–923.

Farra, V., and R. Madariaga, 1988, Nonlinear reflection tomography: Geophysical Journal International, **95**, 135–147.

Goldin, S. V., 1986, Seismic traveltime inversion: SEG.

Koren, Z., I. Ravve, and D. Kosloff, 2006, Curved rays anisotropic tomography: Local and global approaches: 76th Annual International Meeting, SEG, Expanded Abstracts, 3373–3377.

Koren, Z., U. Zackhem, and D. Kosloff, 1999, 3D local tomography — Residual interval velocity analysis on a depth solid model: 69th Annual International Meeting, SEG, Expanded Abstracts, 1255–1258.

Kosloff, D., J. Sherwood, Z. Koren, E. Machet, and Y. Falkovitz, 1996, Velocity and interface depth determination by tomography of depth migrated gathers: Geophysics, **61**, 1511–1523.

Menke, W., 1989, Geophysical data analysis: Discrete inverse theory, rev. ed.: Academic Press, Inc.

Stork, C., 1992, Reflection tomography for the post-migrated domain: Geophysics, **57**, 680–692.

Tarantola, A., 1987, Inverse problem theory: Methods for data fitting and model parameter estimation: Elsevier Science Publishing Co., Inc.

Thomsen, L., 1986, Weak elastic anisotropy: Geophysics, **51**, 1954–1966.

Tsvankin, I., 2001, Seismic signatures and analysis of reflection data in anisotropic media: Elsevier Science Publishing Co., Inc.

Williamson, P. R., 1990, Tomographic inversion in reflection seismology: Geophysical Journal International, **100**, 255–274.